Geology, Fluid Inclusions and Stable Isotopes of the Xialiugou Polymetallic Deposit in North Qilian, Northwest China: Constraints on Its Metallogenesis

Yongjun Shao [1,2], **Huajie Tan** [1,2], **Guangxiong Peng** [1,2], **Jiandong Zhang** [1,2], **Jianzhou Chen** [3], **Qiaomei Chen** [3] **and Yu Zhang** [1,2,*]

[1] Key Laboratory of Metallogenic Prediction of Nonferrous Metals and Geological Environment Monitoring (Central South University), Ministry of Education, Central South University, Changsha 410083, China
[2] School of Geosciences and Info-physics, Central South University, Changsha 410083, China
[3] Qinghai Fourth Geological and Mineral Exploration Institute, Xining 810024, China
[*] Correspondence: zyu2005@csu.edu.cn; Tel.: +86-731-888-30616

Abstract: The Xialiugou polymetallic deposit is located in the North Qilian Orogenic Belt, Northwest China, of which the main ore-bearing strata are the Middle Cambrian Heicigou Group. The mineralization is zoned with "black" orebodies (galena–sphalerite), which are stratigraphically above the "yellow" orebodies (pyrite–chalcopyrite–tennantite) at the lower zone, corresponding to the alteration assemblages of quartz–sericite in the ore-proximal zone and chlorite in the ore-distal zone. The Xialiugou mineralization can be divided into three stages: (1) Stage I (pyrite); (2) Stage II (chalcopyrite–tennantite–sphalerite); and (3) Stage III (galena–sphalerite). Fluid inclusions data indicate that the physicochemical conditions that lead to ore formation were the medium–low temperature (157–350 °C) and low salinity (0.17–6.87 wt % $NaCl_{eqv}$), and that the ore-forming temperature tended to decrease with the successive mineralization processes. Taking the H–O isotopic compositions (δD_{V-SMOW} = −51.0‰ to −40.5‰, $\delta^{18}O_{H2O}$ = −0.4‰ to 8.6‰) into consideration, the ore-forming fluids were most likely derived from seawater with a small amount of magmatic- and meteoric-fluids input. In addition, the combined S (−3.70‰ to 0.10‰) and Pb isotopic ($^{206}Pb/^{204}Pb$ = 18.357 to 18.422, $^{207}Pb/^{204}Pb$ = 15.615 to 15.687, $^{208}Pb/^{204}Pb$ = 38.056 to 38.248) data of pyrite indicate that the ore-bearing volcanic rocks may be an important source of ore-forming materials. Finally, we inferred that the Xialiugou deposit shares similarities with the most important volcanogenic massive sulfide (VMS) deposits (Baiyinchang ore field) in China and typical "black ore" type VMS deposits worldwide.

Keywords: fluid inclusions; stable isotopes; ore-forming source; metallogenesis; Xialiugou deposit; North Qilian Orogenic Belt

1. Introduction

Volcanogenic massive sulfide (VMS) deposits are an important source of copper, lead, and zinc [1]. Previous studies on various Paleozoic to Cenozoic VMS deposits have revealed their most significant features, which primarily include: (1) an extensional geotectonic environment for their formation such as midocean ridges, back-arc basins, continental rifts and island-arcs [2]; (2) zonation from a layered massive sulfide unit to a footwall stockwork mineralization zone [3,4]; (3) extensive and intensive proximal alteration assemblages including quartz, chlorite, white mica (sericite) and pyrite [2,4], (4) moderate-temperature ore-forming fluids derived from heated seawater leaching into the surrounding and underlying volcanic rocks and/or magmatic–hypothermal fluids [2,4].

As one of the most important polymetallic metallogenic zones in China, the North Qilian Orogenic Belt (NQOB) is located on the northeastern edge of the Qinghai–Tibet plateau, adjacent to the Alashan Block in the north, and the Qilian Block in the south (Figure 1a). It is well-known for its abundant metal resources, especially the Early Paleozoic copper polymetallic deposits [5–9]. To date, 12 deposits have been found in the Guomisi–Bailiugou district located in the western region of the NQOB, namely Dongtiegou, Haxionggou, Wuminggou, Xuejigou, Xishanliang, Xialiugou, Wanyanghe, Xiagou, Bailiugoiu, Guomisi, Gadaban and Xiangzigou polymetallic deposits. Since the 1980s, studies on the Guomisi–Bailiugou district have focused on the structural evolution, alteration/mineralization features, and the geochemistry of ore-bearing volcanic rocks [10–16]. However, the ore-forming psychochemical conditions in which the ores are formed and the ore-forming material sources have not been effectively elucidated [10,12,16], meaning that the genesis of ores is unclear.

In this paper, we present a dataset of the fluid inclusions and H–O–S–Pb isotopes from the Xialiugou deposit, coupled with field observations and alteration/mineralization paragenesis, to constrain the origin of the Xialiugou deposit. These new studies can provide better insight into the ore-forming processes in the North Qilian Orogenic Belt.
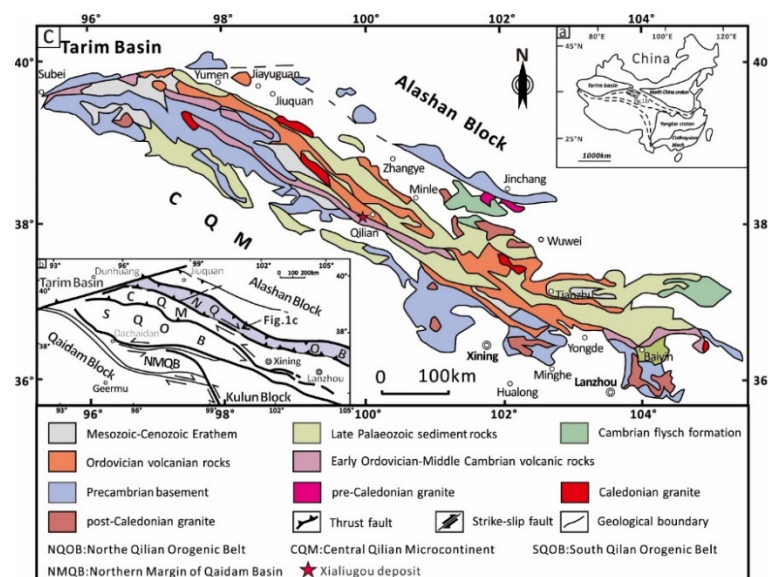
Figure 1. (**a**) Schematic map showing major tectonic units of China; (**b**) tectonic units of North Qilian Orogenic Belt (NQOB); (**c**) geological sketch map of the Northern Qilian, Mountains, modified from reference [7].

2. Regional Geology

The NQOB lies in the middle section of the Qinling–Qilian–Kunlun Giant Orogenic Belt and is surrounded by the Tarim Block, the North China Block, and the middle Qilian–Qaidam Block (Figure 1b). It is an Early Paleozoic Orogenic Belt with a typical trench–arc–basin system. Extending to the NW, it is about 1200 km long and 100–300 km wide [17,18], and is bounded by the dextral Tongxin–Guyuan Fault to the east, the Longshoushan Fault and Alashan Block to the north, the middle Qilian Block to the south, and the sinistral Altun Fault to the west [7] (Figure 1b,c). The NQOB includes a Precambrian metamorphic basement and Paleozoic sedimentary rocks. Precambrian metamorphic basement rocks include the Paleoproterozoic Beidaihe Group, the Zhulongguan and Gaolan Groups of the Changcheng System, and the Jintieshan Group of the Jixian System from the oldest to the youngest. The biotite schist of the Beidaihe Group yielded a whole-rock Sm–Nd age of 1980 ± 0.27 Ma, and the diabase of the Zhulongguan Group yielded a zircon U–Pb weighted average age of 1777 ± 28 Ma [19]. The Neoproterozoic Baiyanghe Group is a sedimentary rock combination of tillites, glutenites, and limestones [20]. The Paleozoic rocks are composed of the Middle Cambrian

volcanic-clastic rocks, the Lower Ordovician Yingou Group, the Middle Ordovician volcanic breccia of the Zhongbao Group, the Upper Ordovician limestones of the Jianmenzi Formation [21], the Silurian shallow marine clastic rocks [22], the Devonian foothills–river–lake facies of calcarenite argillaceous sandstone of the Laojunshan Formation [23], and the Carboniferous-Permian sandstones, shales, and limestones. Most NQOB deposits are hosted by Middle Cambrian and Ordovician volcanic rocks.

The structure of the NQOB is composed of three parallel NWW-trending faults (the Longshou–Gushi Fault, North Qilian north margin Fault, and North Qilian south margin Fault) and one SWW-trending fault (the Altyn Tagh Fault). The Altyn Tagh Fault, that limits the Tarim Basin, cuts the NWW-trending fault. The NWW-trending faults, together with their secondary faults, and SWW-trending fault form the regional basic structural arrangement [24].

Volcanic–magmatic activity occurred periodically from the Proterozoic to the Cenozoic, with a maximum widespread magmatism mainly formed in the Early Paleozoic. The Ordovician intrusive rocks are intermediate to intermediate-felsic, whereas the Silurian intrusive rocks are intermediate-felsic to felsic. These are characterized by fissure eruption and central eruption. The Cambrian and Ordovician volcanic rocks are important ore-bearing strata in the NQOB.

According to the geological setting, ore-bearing strata, and ore-forming elements, the Early Paleozoic polymetallic deposits in the NQOB can be divided into two types [7,8,13,14], namely (1) "Cyprus-type" VMS deposits and (2) "black ore type" VMS deposits. The "Cyprus-type" VMS deposits (e.g., the Shijuli copper deposit, with proven metal reserves of 5177t Cu, and 1069 t Zn of its VI orebody) occur in mafic volcanic rocks from the western NQOB [7,8]. The "black ore type" VMS deposits (e.g., the Baiyinchang polymetallic deposit, including the Zheyaoshan and Huoyanshan orebodies with metal reserves of 1.30 Mt Cu, 0.81 Mt Zn and 0.41 Mt Pb, the Xiaotieshan orebodies with metal reserves of 1.14 Mt Cu + Zn + Pb, and the Tongchanggou orebodies) are associated with the intermediate-felsic volcanic rocks, and mostly occur in the eastern NQOB [5,7,11,21].

3. Ore Deposit Geology

The Xialiugou deposit is in the Guomisi–Bailiugou ore field [11,12]. The exposed strata in the Xialiugou district consists of the ore-hosted Middle Cambrian Heicigou Group, the Upper Carboniferous Yanghugou Formation, the Cretaceous and Quaternary (Figure 2a). The Lower Heicigou Group outcropped in the north of the ore field is mainly comprised of lower basaltic and basaltic tuff, and upper sericite–chlorite schist, quartzite, and serpentinite. The rocks in the Upper Heicigou Group are dominated by lower mafic and felsic volcanic rocks (including basalt, basaltic volcanic breccia, basaltic tuffs, and the upper rhyolitic tuff, rhyolite, and rhyolite volcanic breccia).

The NNW–, NE–NEE-trending faults and the Guomisi–Bailiugou volcanic dome are the main structures (Figure 2a). The NE–NEE-trending faults crosscut the Guomisi–Bailiugou volcanic dome, which is approximately 25 km long and 3 to 4 km wide [26,27]. The northern and southern parts of the volcanic dome are composed of both mafic and felsic volcanic lavas, breccias, and tuff, while the core is only composed of felsic volcanic rock [8,28]. The Xialiugou, Wanyanghe, and Xiagou deposits are in the north of the volcanic dome, and the Guomisi and Gadaban deposits are in the south. The orebodies commonly occur at the contact between the mafic and felsic volcanic rocks [29].

The Xialiugou deposit mainly consists of four NNW-trending orebodies (I, II, III, and IV). The No. I Orebody is the largest, with an average length of 1250 m and width of 9.2 m, respectively. The occurrence of an orebody is commonly parallel to that of the ore-hosting strata (Middle Cambrian Heicigou Group). The Xialiugouo orebodies are commonly zoned with a "black" orebody (galena–sphalerite) in the upper zone and "yellow" orebody (pyrite–chalcopyrite–tennantite) in the lower zone (Figure 2b). The corresponding alteration assemblages are characterized by quartz–sericite in the ore-proximal zone and chlorite in the ore-distal zone.
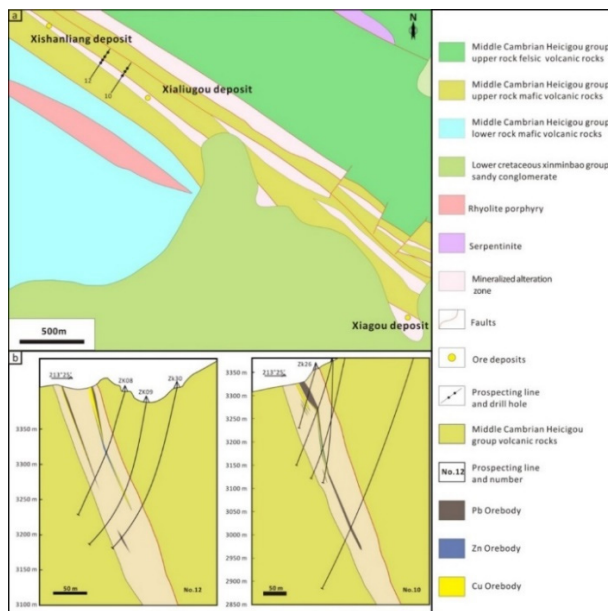
Figure 2. Simplified geological map (**a**) and cross-sectional map of line No.10 (right) and No.12 (left) in the Xialiugou deposit (**b**), m = modified from reference [25].

On the basis of the cross-cutting relationships and minerals assemblages, the mineralization at Xialiugou can be divided into three stages (Figures 3 and 4), namely Stage I (vein–veinlet and disseminated pyrite) (Figure 3a,b); Stage II (vein, disseminated, and layered chalcopyrite–tennantite–sphalerite) (Figure 3c,d); and Stage III (layered, and massive galena–sphalerite) (Figure 3e,f).

Stage I is dominated by a large amount of pyrite, primarily occurring as vein–veinlet and disseminated (Figure 3b) and subhedral grains (mainly 100–300 μm in size; Figure 5a).

Stage II is the main stage of copper mineralization and is dominated by abundant chalcopyrite and tennantite with a minor amount of sphalerite, covellite, bornite, and pyrite (Figure 5b). Chalcopyrite, tennantite and sphalerite commonly occur as anhedral grains. Locally, it can be observed that the pyrite was evidently replaced and filled by chalcopyrite, tennantite and sphalerite (Figure 5c,d). Moreover, pyrite and chalcopyrite are commonly subjected to deformation (Figure 5h).

Stage III is characterized by large amounts of galena and sphalerite with minor amounts of chalcopyrite, tennantite (Figure 5e), bornite, covellite and pyrite (Figure 5f). The sulfides commonly occur as layered and massive (Figure 3f). Locally, the Stage II mineral assemblage of chalcopyrite–tennantite–sphalerite occurs as irregular breccia, cemented by the Stage III mineral assemblage of galena–sphalerite. Additionally, chalcopyrite commonly coexists with sphalerite in the form of disease texture (Figure 5g).

Additionally, the post-mineralization tectonic activity has evidently reworked the orebodies, which have locally caused the orebodies and minerals to be subjected to deformation. In detail, the pyrite behaved in a brittle manner, whereas chalcopyrite, galena, tennantite and/or sphalerite behaved in a ductile manner. The fractured pyrite was sealed with ductile minerals of chalcopyrite, galena, tennantite and/or sphalerite (Figure 5h,i).
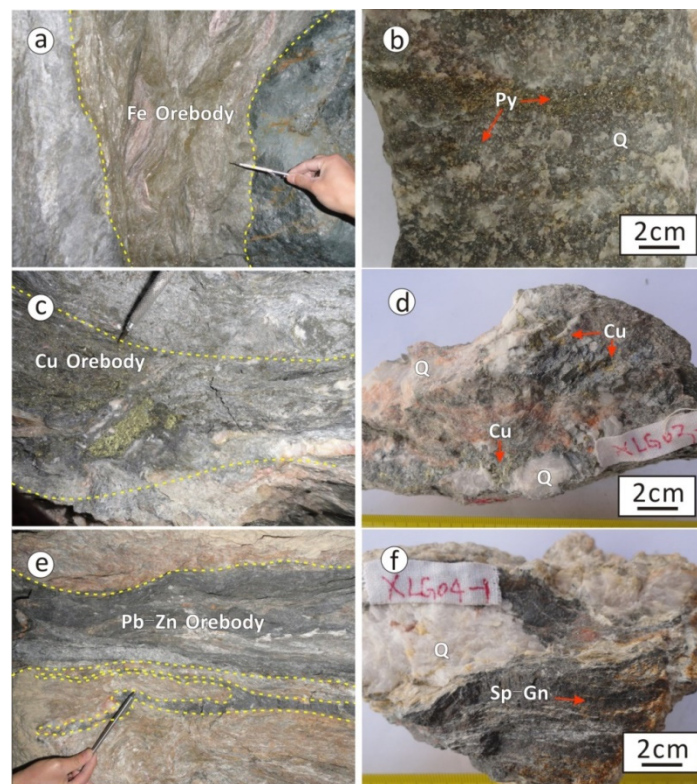
Figure 3. Photographs of orebody and hand specimens showing the mineralization and ore of the Xialiugou deposit. (**a**) Disseminated Fe ore body; (**b**) disseminated pyrite; (**c**) disseminated Cu ore body; (**d**) disseminated chalcopyrite–tennantite–sphalerite; (**e**) massive Pb–Zn ore body; (**f**) layered galena, sphalerite and chalcopyrite. Py = Pyrite; Ccp = Chalcopyrite; Sp = Sphalerite; Gn = Galena. Yellow dashed lines offer demarcation of the ore body within the wallrock or strata.
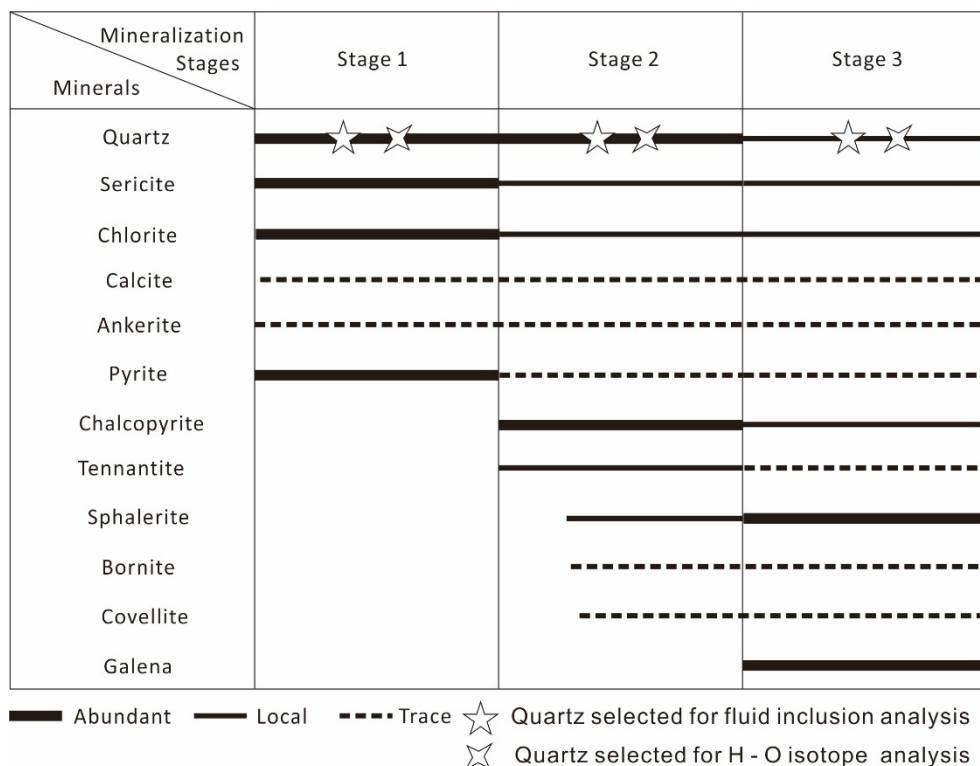
Figure 4. The mineralization stages and paragenetic sequences of the Xialiugou deposit.
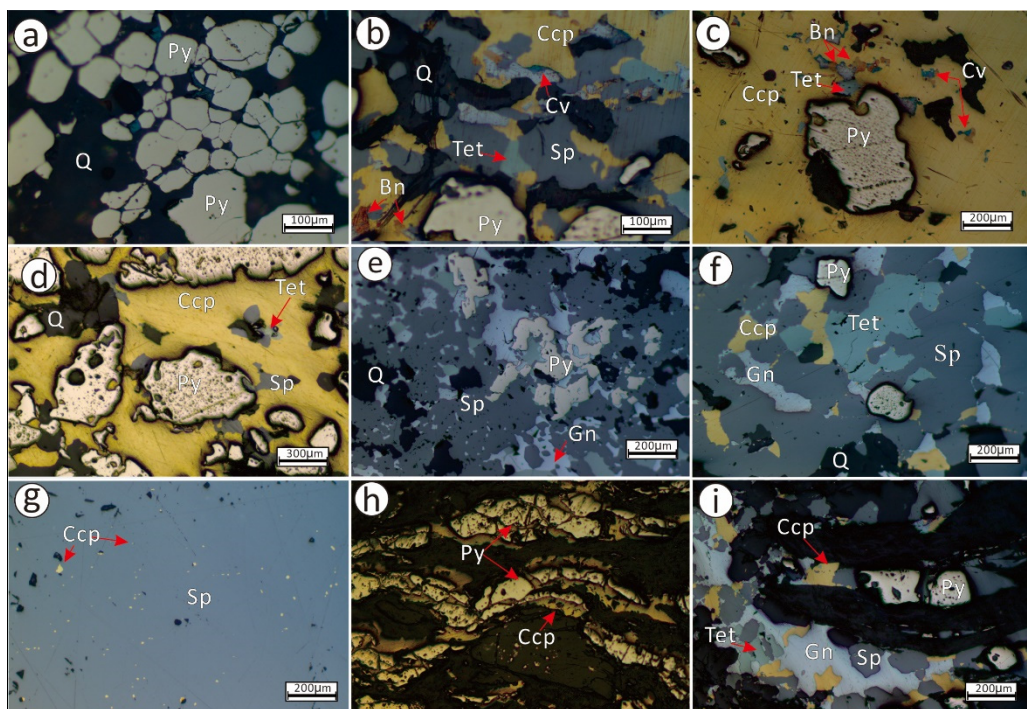
Figure 5. Photomicrographs (reflected light and transmission light) showing the representative mineral assemblages and textural features of the Xialiugou deposit. (**a**) Subhedral crystals in pyrite aggregates. (**b**) The intergrowths of chalcopyrite, tennantite, sphalerite, covellite and bornite that partly replace the subhedral pyrite. (**c**) Pyrite was replaced by chalcopyrite and tennantite as subhedral grains. (**d**) Subhedral pyrite was replaced by chalcopyrite, tennantite and sphalerite. (**e**) The intergrowth of galena and sphalerite partly replaced the subhedral pyrite. (**f**) The intergrowths of galena, sphalerite, chalcopyrite, tennantite, partly surrounded the subhedral pyrite. (**g**) Chalcopyrite coexisting with sphalerite in the form of disease texture. (**h**) Cataclastic texture of pyrite grains sealed by chalcopyrite. (**i**) Pyrite is sealed by ductile minerals of chalcopyrite, galena, tennantite and/or sphalerite. Py = pyrite; Ccp = chalcopyrite; Sp = sphalerite; Tet = tennantite; Bn = bornite; Cv = covellite; Gn = galena; Q = quartz.

4. Samples and Analytical Methods

4.1. Sampling

Ten quartz-bearing samples were collected from the underground mining platform for the No. I Orebody at an elevation of 3430 m, and six and four samples covered every mineralization stage for which the fluid inclusions and H–O analysis were conducted, respectively. Additionally, five pyrite samples corresponding to three mineralization stages for S–Pb isotope analysis were also collected from the No. I Orebody in the underground platform at an elevation of 3430 m.

4.2. Microthermometry of Fluid Inclusions

Petrographic characteristics of the fluid inclusions were performed by optical microscopy on double-section polished thin sections (thicknesses of about 0.06–0.08 mm). Microthermometric measurements of the fluid inclusions were undertaken using a Linkam THMSG 600 heating–freezing stage (−196 °C to 600 °C) at the Key Laboratory of Metallogenic Prediction of Nonferrous Metals and Geological Environment Monitoring (Central South University, Changsha, China). The measurements had a precision better than ±1 °C and ±0.1 °C at the temperature range of 30 °C to 600 °C and −196 °C to 30 °C, respectively. Freezing and heating temperatures were measured using the same inclusion where possible, and phase transitions were monitored carefully. During the temperature measurement process, temperatures were changed in steps of 5 to 10 °C/min, and then changed slowly at steps of 0.1

to 1 °C/min when approaching the temperature of the phase transition. According to the results of the final melting temperature of ice and the vapor–liquid two-phase total homogenization temperature by the heating–freezing table, the salinity and the density of the aqueous solution were calculated by the FLINCOR computer program developed by Brown (Version 1.4, Department of Geology and Geophysics University of Wisconsin-Madison, Madison, WI, USA) [30].

4.3. H–O Isotope Analysis

The H–O isotope analyses were performed at the Analytical Test Center of the Beijing Institute of Geological Sciences (Beijing, China) using a Finnigan-MAT253 mass spectrometer. Every stage of the quartz grains for H–O isotope analysis was separated using a magnetic separator from the quartz-bearing samples of the corresponding mineralization stage [31,32]. Oxygen was liberated from quartz by reaction with BrF_5 and converted to CO_2 on a platinum-coated carbon rod for the oxygen isotope analysis [33]. The samples used to measure the hydrogen isotopes were first degassed of unstable volatiles by heating at 150 °C for 3 h under a vacuum. The water in the quartz samples was released by heating the samples to approximately 500 °C in an induction furnace and then reacted with zinc powder at 410 °C to generate hydrogen for the hydrogen isotope analysis [32]. The results are reported in per per milliliter, relative to V-SMOW standards, and the precision was ±2‰ for δD and ±0.2‰ for $\delta^{18}O$ [34].

4.4. S and Pb Isotope Analytical Methods

The S and Pb isotope analyses were performed at the Analytical Test Center of the Beijing Institute of Geological Sciences. The samples were selected, crushed, and processed. Pure single mineral (>95%) was selected for isotopic analysis. The S isotope analyses were performed using a MAT-251 mass spectrometer. Cu_2O was used as the oxidizer to react with the sulfide to produce SO_2, which was frozen and collected for S isotopic analysis [35]. The international standard V_{CDT} was adopted. The accuracy was ±0.2‰. The Pb isotope was determined by an IsoProbe-T thermal ionization mass spectrometer (TIMS). Pb was separated and purified using a conventional cation-exchange technique (AG1×8, 200–400 resin) with diluted HBr as the eluent. The $^{206}Pb/^{204}Pb$, $^{207}Pb/^{204}Pb$, and $^{208}Pb/^{204}Pb$, ratios of the NBS981 Pb standard were 16.940 ± 0.010 (±2σ), 15.498 ± 0.009 (±2σ), and 36.716 ± 0.023 (±2σ), respectively. The detailed analytical method and procedures can be found in [36].

5. Results

5.1. Fluid Inclusions

5.1.1. Fluid Inclusions Classifications and Characteristics

Petrographic observations indicate that the fluid inclusions were widely distributed in quartz. The petrography of the fluid inclusions was conducted in accordance with the following rules: the isolated fluid inclusions and randomly distributed groups of fluid inclusions hosted in quartz crystals were interpreted as primary in origin, and those aligned along micro-fractures in the transgranular trails were interpreted as secondary [37,38].

In terms of the number and volumetric proportions of the phases present in the fluid inclusions at room temperature, two major types of primary or pseudosecondary inclusions could be recognized in the Xialiugou deposit: two-phase liquid-rich fluid inclusions (I_a), two-phase vapor-rich fluid inclusions (I_b), and no pure liquid phase or CO_2 inclusions or daughter mineral-bearing aqueous inclusions. Two-phase liquid-rich fluid inclusions (I_a) and two-phase vapor-rich fluid inclusions (I_b) were present in all stages, and two-phase liquid-rich fluid inclusions were predominant by more than 95%.

Two-phase liquid-rich fluid inclusions (I_a): this type of fluid inclusion consists of a vapor bubble and a liquid phase, with a high degree of fill (Vl/(Vl + Vg) > 0.6). They ranged in size from approximately

4 to 17 μm and were mostly nearly ellipsoidal (Figure 6a), irregular (Figure 6b) and negative crystals. These fluid inclusions homogenized to the aqueous phase.

　　Two-phase vapor-rich fluid inclusions (I_b): this type of fluid inclusion consists predominantly of vapor, with a low degree of fill (Vl/(Vl + Vg) < 0.5). Ellipsoidal (Figure 6c), irregular (Figure 6d), and negative crystals were observed, and their sizes ranged from 8 to 11 μm. These fluid inclusions homogenized to the aqueous phase.
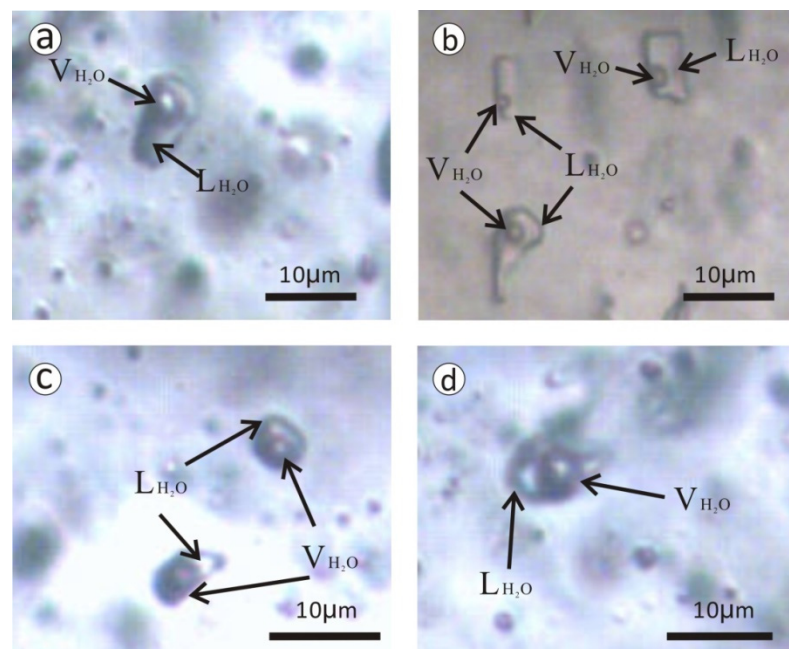
Figure 6. Photomicrographs of fluid inclusions types from the Xialiugou deposit. The two-phase liquid-rich fluid inclusions (I_a) were near ellipsoidal (**a**), and irregular (**b**); the two-phase vapor-rich fluid inclusions (I_b) were near ellipsoidal (**c**), and irregular (**d**). L_{H2O} liquid H_2O, V_{H2O} vapor H_2O.

5.1.2. Microthermometric Data of Fluid Inclusions

　　Microthermometric studies were conducted on the primary inclusions from the three stages. The microthermometric data of fluid inclusions are summarized in Table 1 and Figure 7.

　　Stage I: The fluid inclusions in quartz were mainly liquid-phase-dominated inclusions (I_a), and a small amount were vapor-phase-dominated inclusions (I_b). The homogenization temperature was 223 to 350 °C (Figures 7a and 8a) and was mainly concentrated at 270 to 325 °C; the salinity was 0.17 to 3.44 wt % $NaCl_{eqv}$ (Figures 7b and 8a); the density is 0.569 to 0.848 g/cm^3.

Table 1. Microtemperature measurements of the primary inclusions in different mineralization stages of exhalative-sedimentary periods from the Xialiugou deposit.

| Sample	Stage	Nub	Size (μm)	Vapor–Liquid Ratio (%)	Tm_{ice} (°C)	Th_{total} (°C)	Salinity (wt % $NaCl_{eqv}$)	Density (g/cm^3)
XLG5-5	I	15	5.0–13.0	18–50	−2.1 to −0.1	262–350	0.17–3.44	0.569–0.793
XLG11-2		15	4.3–12.0	17–35	−1.8 to −0.1	223–311	0.17–3.05	0.670–0.848
XLG3-5	II	20	4.7–14.5	5–30	−3.3 to −0.6	191–334	0.18–5.40	0.689–0.892
XLG8-10		15	5.7–12.1	8–50	−4.3 to −1.9	210–294	3.21–6.87	0.780–0.893
XLG4-1	III	15	4.1–9.4	13–45	−1.6 to −0.1	169–241	0.18–2.72	0.832–0.921
XLG8-7		14	4.5–9.7	16–38	−6.0 to −0.2	157–182	0.33–5.47	0.900–0.973

Nub: the number of measured fluid inclusions; Tm_{ice}: the final melting temperature of ice; Th_{total}: the temperature of total homogenization.

Stage II: The fluid inclusions in quartz were dominated by liquid-phase-dominated inclusions (I_a), and also contained several small amounts of vapor-phase-dominated inclusions (I_b). The homogenization temperature was 191 to 334 °C (Figures 7c and 8a), mainly concentrated at 210 to 270 °C; the salinity was 0.18 to 6.87 wt % $NaCl_{eqv}$ (Figures 7d and 8a); the density was 0.689 to 0.893 g/cm³.

Stage III: The fluid inclusions in quartz were mainly liquid-phase-dominated inclusions (I_a), and a small amount were vapor-phase-dominated inclusions (I_b). The homogenization temperature was 157 to 241 °C (Figures 7e and 8a), mainly concentrated at 150 to 200 °C; the salinity was 0.18 to 5.47 wt % $NaCl_{eq\,v}$ (Figures 7f and 8a); the density was 0.832 to 0.973 g/cm³.
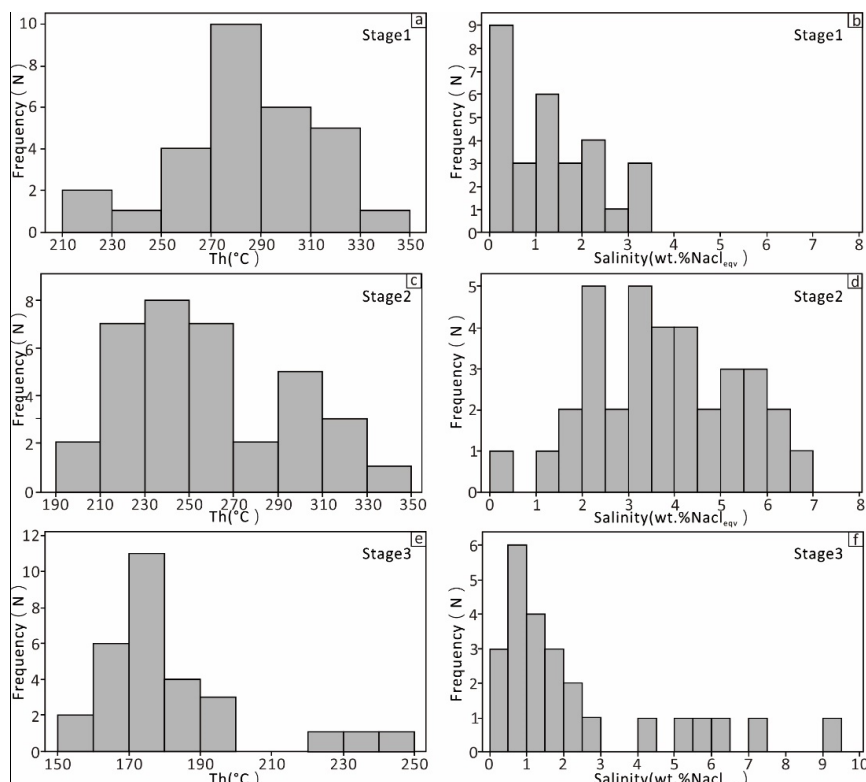
Figure 7. Histograms of the homogenization temperatures (**a**,**c**,**e**) and salinities (**b**,**d**,**f**) of the fluid inclusions in the Xialiugou deposit.
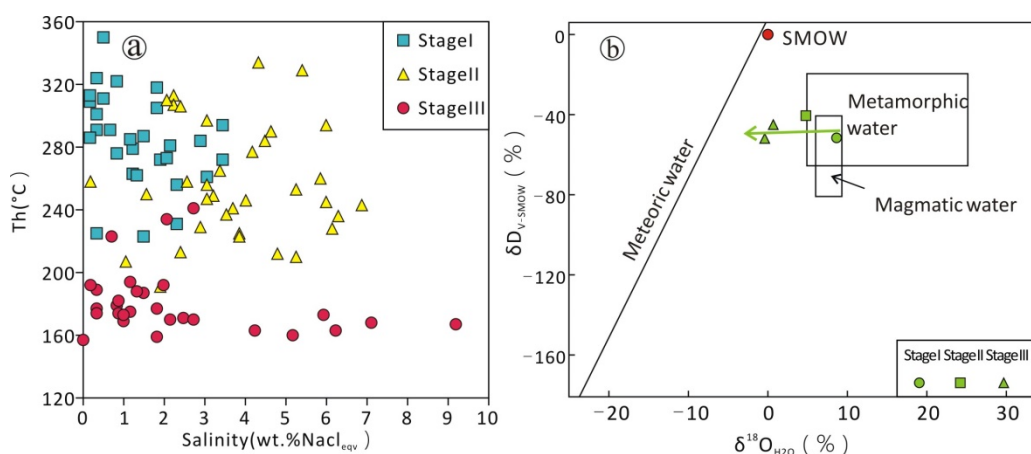
Figure 8. The temperature and salinity diagram of the Xialiugou deposit (**a**); $\delta D_{v\text{-smow}}$ and $\delta^{18}O_{H2O}$ diagram for fluids of the Xialiugou deposit (**b**), modified from references [40,41].

5.2. Isotope Geochemistry

5.2.1. H–O Isotopes

The results of the H–O isotope test are shown in Table 2. The $\delta^{18}O_{H2O}$ values were calculated using the fractionation equation: $1000\ln\alpha \approx 3.38 \times 10^6/T^2 - 3.40$ [39], where "α" is the fractionation factor and "T" is the homogenization temperature of fluid inclusions for each mineralization stage.

In the Xialiugou deposit, the $\delta D_{V\text{-}SMOW}$ and $\delta^{18}O_{H2O}$ values of ore-forming fluids in Stage I were −51.6‰ and 8.6‰, respectively, corresponding to the $\delta^{18}O_{V\text{-}SMOW}$ value of 15.0‰ (Figure 8b). The Stage II $\delta D_{V\text{-}SMOW}$ and $\delta^{18}O_{H2O}$ values of ore-forming fluids were −40.5‰ and 4.8‰, respectively, which corresponded to the $\delta^{18}O_{V\text{-}SMOW}$ value of 14.1‰ (Figure 8b). The Stage III $\delta D_{V\text{-}SMOW}$ and $\delta^{18}O_{H2O}$ values of the ore-forming fluids ranged from −51.9‰ to −40.5‰ and −0.4‰ to 4.1‰, respectively, which corresponded to the $\delta^{18}O_{V\text{-}SMOW}$ values of 13.5‰ to 13.7‰ (Figure 8b).

Table 2. The $\delta D_{V\text{-}SMOW}$ and $\delta^{18}O_{V\text{-}SMOW}$ values of the fluid inclusions in quartz, and calculated values for equilibrium fluids from the Xialiugou deposit.

Sample No.	Mineral	$\delta D_{V\text{-}SMOW}$(‰)	$\delta^{18}O_{V\text{-}SMOW}$(‰)	$\delta^{18}O_{H2O}$(‰)	T (°C)	Stage
XLG5-3	Quartz	−51.6	15.0	8.64	315	I
XLG3-5	Quartz	−40.5	14.1	4.78	242	II
XLG8-11	Quartz	−45.0	13.5	0.68	183	III
XLG8-2	Quartz	−51.9	13.7	−0.40	166	III

5.2.2. S Isotope

The S isotopic data are listed in Table 3. The $\delta^{34}S$ isotope values ranged from −3.70‰ to 0.10‰, with an average of −1.32‰. The $\delta^{34}S$ isotope values are −1.60‰, −1.20‰ to 0.10‰, and −0.20 to −3.70‰, for Stage I, II, III, respectively. The $\delta^{34}S$ values in Stage III were slightly higher than Stage I and III, but all of the $\delta^{34}S$ values were close to 0‰.

Table 3. $\delta^{34}S_{V\text{-}CDT}$ values of the Xialiugou deposit.

Sample No.	Mineral	$\delta^{34}S_{V\text{-}CDT}$(‰)	Stage
XLG4-3	Pyrite	−1.60	I
XLG6-1	Pyrite	−1.20	II
XLG7-1	Pyrite	0.10	II
XLG8-7	Pyrite	−0.20	III
XLG9-3	Pyrite	−3.70	III

5.2.3. Pb Isotope

The Pb isotopic data are listed in Table 4, which shows that the $^{206}Pb/^{204}Pb$, $^{207}Pb/^{204}Pb$ and $^{208}Pb/^{204}Pb$ values of pyrite were 18.357 to 18.422, 15.615 to 15.687, and 38.056 to 38.248, respectively. The $^{206}Pb/^{204}Pb$, $^{207}Pb/^{204}Pb$ and $^{208}Pb/^{204}Pb$ values for all stages were similar, and the values of Stage III were slightly higher than Stage I and II.

Table 4. The lead isotope values of the Xialiugou deposit.

Sample No.	Mineral	$^{206}Pb/^{204}Pb$	$^{207}Pb/^{204}Pb$	$^{208}Pb/^{204}Pb$	μ	ω	k	Stage
XLG4-3	Pyrite	18.345	15.653	38.168	9.58	36.25	3.66	I
XLG6-1	Pyrite	18.381	15.642	38.143	9.55	35.85	3.63	II
XLG7-1	Pyrite	18.357	15.615	38.056	9.50	35.38	3.60	II
XLG8-7	Pyrite	18.422	15.687	38.248	9.63	36.48	3.67	III
XLG9-3	Pyrite	18.398	15.661	38.163	9.59	36.01	3.63	III

The values of μ, ω, and k were calculated according to reference [42].

6. Discussion

6.1. Characteristics and Source of Ore-Forming Fluids

The H–O isotopic compositions of hydrothermal quartz are effective tracers to determine the sources of ore-forming fluids [41]. Previous studies have indicated that the magmatic hydrothermal fluids commonly are enriched $\delta^{18}O$ (>5‰) [43]. The Stage I quartz is plotted in both magmatic- and metamorphic-fluids zones in the $\delta D_{V\text{-SMOW}}$-$\delta^{18}O_{H2O}$ diagram (Figure 8b), and its $\delta^{18}O_{H2O}$ was markedly higher than 5‰. These results indicate that the sources of part of the initial ore-forming fluids at Xialiugou may have been magmatic hydrothermal fluids. The $\delta^{18}O_{H2O}$ values in Stage II and III were lower than those in Stage I, and lay within the compositional ranges between magmatic and seawater, but shifted towards the meteoric regime, indicating that the ore-forming fluids involved a certain amount of meteoric water.

As the mineralization at Xialiugou formed at or near the seafloor in a volcanic island arc environment [44,45], the contribution of seawater may have been a crucial component of the ore-forming fluids. Additionally, the ore-forming fluids had the characteristics of medium–low temperature (157 to 350 °C) and low salinity (0.17 to 6.87 wt % $NaCl_{eqv}$ < 10 wt % $NaCl_{eqv}$) with only two-phase liquid-rich and vapor-rich fluid inclusions. These characteristics indicate that the main ore-formation process may have derived from the evolved seawater, and are consistent with typical VMS deposits (100 to 360 °C, and 1.9 to 9.1 wt % $NaCl_{eqv}$, and liquid–vapor two-phase fluid inclusions predominantly) [46–49]. Based on the fluid inclusions investigation and H–O isotopic compositions, we propose that the main ore-bearing fluids were most likely derived from evolved seawater, and that a small amount of magmatic water and meteoric water may be an additional component in the ore-forming processes. The characteristics of the ore-forming fluids were, in essence, similar to those of the ore-forming fluids of the Paleozoic VMS-type copper deposits in the Zoulangnanshan area of the NQOB [50] and the Baiyinchang ore field [51,52].

6.2. Ore-Forming Material Source

The S and Pb isotopic studies provide an efficient tool to determine and trace the origin of these components in ore deposits [53,54]. The mineral composition of the Xialiugou deposit is relatively simple and pyrite can be found in three stages. Therefore, the $\delta^{34}S_{V\text{-CDT}}$ value of the sulfides can be used to represent the sulfur composition of the hydrothermal system. The S isotopic analysis results showed that the $\delta^{34}S_{V\text{-CDT}}$ value was in the narrow range of −3.7‰ to 0.1‰ (Figure 9a), suggesting that the sulfur may have been derived from a single source. The $\delta^{34}S_{V\text{-CDT}}$ values of sulfides from the Xialiugou deposit, close to zero, were similar with those of the Baiyinchang VMS ore field (Figure 9b) [51,55], and the adjacent Gadaban and Gomisi deposits (Figure 9b) [45] where it was inferred that sulfur possibly originated from the underlying volcanic rocks. Meanwhile, the ore-bearing volcanic rocks were strongly altered at Xialiugou. Therefore, the sulfur may have been more or less contributed by the ore-bearing volcanic rocks, which were leached by the hydrothermal system.

Compared to the light stable isotopes, Pb isotopes are not prone to the effects of physical fractionation and are, therefore, considered to be the best way to reflect the source of lead in ore [56]. Due to differences in the locations of ore-forming structures, ore-forming environments, and ore-bearing surrounding rock, the Pb isotope has different characteristics [57–61]. The radiogenic Pb of sulfides after their formation is negligible since they have very low U and Th contents. The ratios of $^{206}Pb/^{204}Pb$, $^{207}Pb/^{204}Pb$, and $^{208}Pb/^{204}Pb$ of the pyrite from the Xialiugou deposit varied in a narrow range from 18.357 to 18.422, 15.615 to 15.687, and 38.056 to 38.248, respectively. Lead with high μ values (>9.58) was derived from the upper crust, whereas lead with μ values of 8.92 was derived from the mantle [42]. Sulfides from the Xialiugou deposit yielded μ values of 9.50 to 9.63, indicating that the lead had a crustal and mantle source. In the $^{207}Pb/^{204}Pb$–$^{206}Pb/^{204}Pb$ and $^{208}Pb/^{204}Pb$–$^{206}Pb/^{204}Pb$ diagram (Figure 10a,b), the data spots were mainly concentrated between the orogenic belt line and upper crust line. Moreover, the data spots were also distributed within the range of the Baiyinchang

VMS-type ore field and had similar characteristics (Figure 10a,b) [51,55]. The orogenic belt (island arc) Pb is considered to be a mixture of crust and mantle-sourced lead [42,62]. The Pb was derived from a mixed upper-crust-orogenic source. Meanwhile, the ore-bearing volcanic rocks also had the characteristics of lower crust and mantle source (^{87}Sr/^{86}Sr = 0.7042, ^{87}Sr/^{86}Sr = 0.7129) [21], showing that the mineralization was related to the ore-bearing volcanic rocks. The ore-bearing volcanic rocks may be an important source of ore-forming materials.
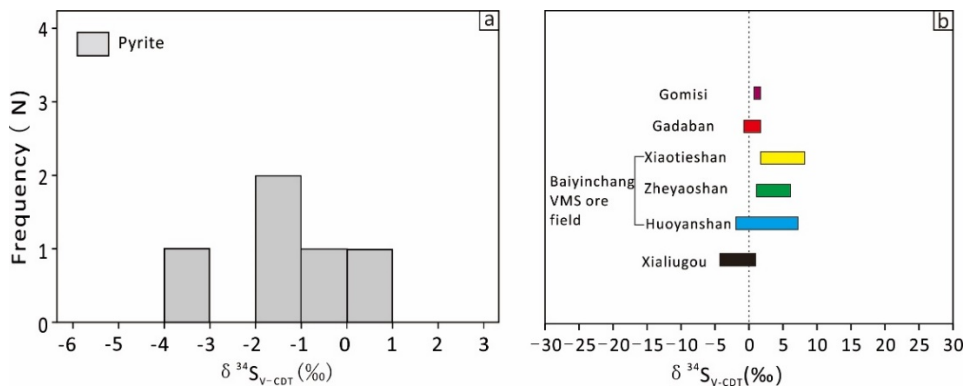
Figure 9. Histogram (**a**) and distribution (**b**) of δ^{34}S$_{V-CDT}$ values for sulfide minerals from the Xialiugou deposit. Dates for Huoyanshan, Zheyaoshan, and Xiaotieshan deposit cited from [51,55]; dates for Gadaban and Gomisi deposit cited from [45].
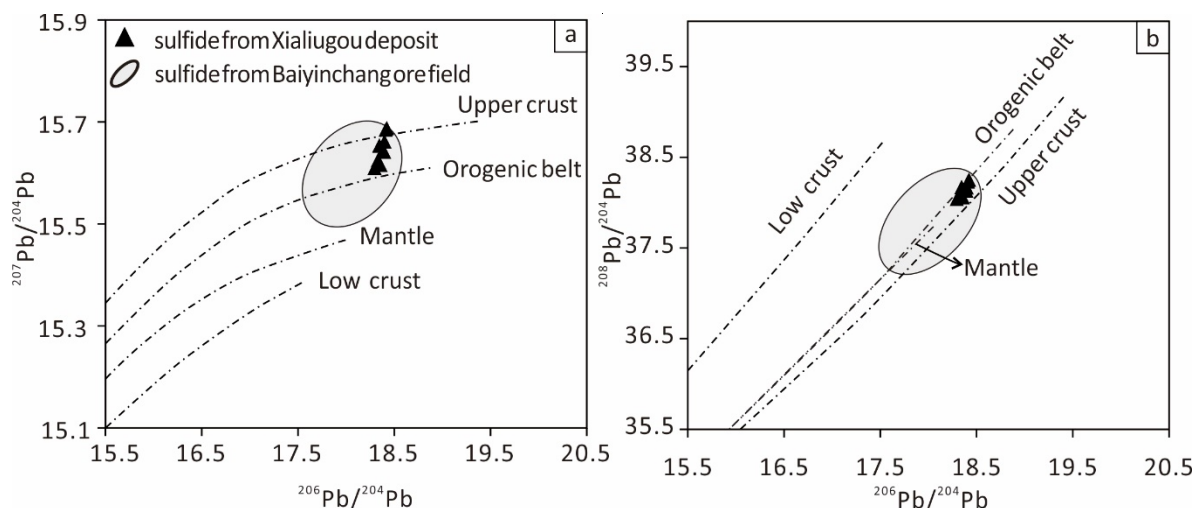
Figure 10. The ^{207}Pb/^{204}Pb–^{206}Pb/^{204}Pb (**a**) and ^{208}Pb/^{204}Pb–^{206}Pb/^{204}Pb (**b**) diagrams of the Pb isotopic compositions for sulfide minerals (pyrite) from the Xialiugou deposit, modified from reference [42]. Data for Baiyinchang ore field cited from [51,55].

6.3. Metallogenesis

The North Qilian, where Xialiugou deposit is located, underwent a complex tectonic evolution [45]. From the Mid-Late Neoproterozoic to the Early Cambrian period (660–540 Ma), the Rodinia supercontinent broke up, and the Northern Qilian Ocean and Southern Qilian Ocean opened and expanded. The Northern Qilian Ocean continued to expand during the Early- and Mid-Cambrian period (540–520 Ma) and the southern margin of the Alashan Block changed from the passive continental margin to the active continental margin due to oceanic subduction. The Early Paleozoic oceanic lithosphere subducted northward at a low angle beneath the Alashan Block, leading to island arc volcanism. As the subduction continued, a complex trench-arc-basin system started to develop on the north of the North Qilian Ocean and the southern margin of the Alashan block (520–446 Ma), and formed a complete trench–arc–basin system in the late Ordovician period (446 Ma). The zircon

U–Pb age of the ore-bearing volcanic rocks of Xialiugou was 503 ± 3 Ma [29], indicating that the mineralization developed in the Late Cambrian period. Moreover, the latest field mapping and volcanic rock geochemistry of the Guomisi–Bailiugou ore field indicate that the tectonic setting is a volcanic island arc environment [44,45] similar to the kuroko VMS-type "black-ore" deposits in Japan.

On the basis of the geological characteristics, fluid inclusions, and the isotopic data, the Xialiugou deposit shares some similarities with the most important Chinese VMS deposits (Baiyinchang ore field) and the typical "black ore" type VMS deposit. These features include: (1) the deposit occurring in the volcanic island arc environment; (2) the ores being zoned with upper layered "black" orebodies (galena–sphalerite) and lower veins "yellow" orebodies (pyrite–chalcopyrite–tennantite); (3) the ore-forming fluids with the characteristics of medium–low temperature and, low salinity in which the main ore-forming fluids may be mainly derived from the evolved seawater; (4) the ore-forming metals may have been derived from the ore-bearing volcanic rocks. The mineralization of the Xialiugou deposit was a continuous process, and the lower channel phase and the upper sedimentary phase orebodies developed in the same hydrothermal system.

The metallogenesis of the Xialiugou deposit can be interpreted as follows. Under the tectonic setting of strong oceanic crust subduction, a large number of submarine volcanic activities took place in the Xialiugou district. The underplating of the deep magma occurred during the interval of volcanic activity or in the late stage of acidic volcanism. Meanwhile, the infiltrated seawater was absorbed into the volcanic channel along the fractures due to the decompression of the shallow magma chamber caused by the volcanic eruption and leached the ore-forming materials from the underlying volcanic rocks and the surrounding volcanic rocks. The circulating seawater may mix with a small part of the magmatic fluids and ore-forming metals. In the early stage, ore-forming fluids flowed upward along the fracture system of the volcanic channels or volcanic structures (open and semi-open system), with the invasion of shallow or ultra-shallow subvolcanic rocks. When the temperature of the ore-forming fluids dropped to 223–350 °C, the salinity was 0.17–3.44 wt % $NaCl_{eqv}$, and the density was 0.569–0.848 g/cm^3, and a large amount of pyrite precipitated from the hydrothermal fluids to form disseminated, vein-like, reticulate orebodies through filling and metasomatic replacement. In the middle stage, the ore-forming hydrothermal fluids continued to move upwards. When the temperature range of the ore-forming fluids was 191–334 °C, the salinity was 0.18–6.87 wt % $NaCl_{eqv}$, and the density was 0.689–0.893 g/cm^3, amounts of the chalcopyrite, tennantite and minor sphalerite began to precipitate from the hydrothermal fluids and formed vein-like and disseminated orebodies. The layered and massive orebodies could be seen locally. In the late stage, the ore-bearing fluids migrated upward along the hydrothermal recharge channel, driven by the subvolcanic hydrothermal system. Furthermore, the ore-bearing fluids were vented from the seafloor and mixed with the meteoric water. The temperature of the ore-forming fluids dropped significantly. When the temperature decreased to 157–241 °C, the salinity decreased to 0.18–5.47 wt % $NaCl_{eqv}$, and the density was 0.832–0.973 g/cm^3, as the layered, massive galena–sphalerite orebodies formed at the top of the deposit. These changes in the physico-chemical conditions and the compositions of the ore-forming fluids during their ascent along the faults and fracture networks to the seafloor played important roles in the ore-forming processes of the layered massive orebodies. After the formation of the Xialiugou deposit, the submarine volcanic activity was renewed, and subsequently, produced more volcanic rocks that covered and preserved the deposit.

7. Conclusions

1. The Xialiugou mineralization was hosted in the volcanic rocks (the Middle Cambrian Heicigou Group), between the mafic and felsic volcanic rocks. The orebodies showed a dual-layered structure with "black" orebodies (galena–sphalerite) on the upper zone and "yellow" orebodies (pyrite–chalcopyrite–tennantite) in the lower zone, showing a typical feature of VMS type deposit of "upper layered and lower veins".

2. The mineralization at Xialiugou could be divided into three stages: Stage I (vein–veinlet and disseminated pyrite), Stage II (vein, disseminated, and layered chalcopyrite–tennantite–sphalerite), and Stage III (layered, and massive galena–sphalerite). The corresponding alteration assemblages were characterized by quartz–sericite in the ore-proximal zone and chlorite in the ore-distal zone.

3. The microthermometry of the fluid inclusions and the H–O isotopic data indicate that the ore-forming fluids had the characteristics of medium–low temperature, and low salinity; the main components of the ore-forming fluids were probably from the evolved seawater and a small amount of magmatic and meteoric fluids may be involved the ore-forming processes. The S and Pb isotopic data revealed that the ore-bearing volcanic rocks may be an important source of ore-forming materials.

4. The Xialiugou deposit can be interpreted as a "black ore" type VMS deposit.

Author Contributions: Y.S., Y.Z., H.T., G.P., J.Z., J.C. and Q.C. conceived and designed the experiments; Y.Z. and H.T. carried out the experiments; Y.S., Y.Z. and H.T. helped to edit and improve the English language and style; and all authors completed the paper.

Conflicts of Interest: The authors declare no conflict of interest.

References

1. Hannington, M.D.; de Ronde, C.E.J.; Petersen, S. *Seafloor Tectonics and Submarine Hydrothermal Systems*; Economic Geology 100th Ann; Society of Economic Geologists: Littelton, CO, USA, 2005; pp. 111–141.

2. Piercey, S.J. The setting, style, and role of magmatism in the formation of volcanogenic massive sulfide deposits. *Miner. Depos.* **2011**, *46*, 449–471. [CrossRef]

3. Cook, N.J.; Klemd, R.; Okrusch, M. Sulphide mineralogy, metamorphism and deformation in the Matchless massive sulphide deposit, Namibia. *Miner. Depos.* **1994**, *29*, 1–15. [CrossRef]

4. Zheng, Y.; Wang, Y.J.; Chen, H.Y.; Lin, Z.W.; Hou, W.S.; Li, D.F. Micro-textural and fluid inclusion data constraints on metallic remobilization of the Ashele VMS Cu-Zn deposit, Altay, NW China. *J. Geochem. Explor.* **2016**, *171*, 113–123. [CrossRef]

5. Peng, L.G.; Ren, Y.X.; Li, Z.P. *The Metallogenic Model of Copper Polymetallic Deposit in Baiyinchang, Gansu Province*; Geological Publishing House: Beijing, China, 1995. (In Chinese)

6. Feng, Y.M. *Geotectonics and Orogeny of the Qinling Mountains, China*; Geological Publication House: Beijing, Chine, 1996; pp. 1–135. (In Chinese)

7. Li, W.Y. *Metallogenesis and Prospecting of Metal Sulfide Deposits Related to Magmatic Action in Qilian Mountain*; Geological Publishing House: Beijing, China, 2006. (In Chinese)

8. Jia, Z.Q. *Metallogenic Regularity and Metallogenic Prediction of Copper-Gold-Tungsten-Lead-Zinc Deposits in Qilian Mountain*; Geological Publishing House: Beijing, China, 2007. (In Chinese)

9. Qi, Z.L.; Li, Y.Y. Investigation on the forming reason of the copper multi-metal deposit in the Xialiugou-Gadaban area of Northen Qilian. *J. Qinghai Univ.* **2010**, *28*, 37–41. (In Chinese)

10. Wu, J.R.; Yu, P.S.; Huang, Y.C. Analysis for metallogenic and geological condition of copper-multi-metal in Qingshuigou to Bailiugou region, North Qilian. *Northwest Geosci.* **1995**, *16*, 50–68. (In Chinese)

11. Hou, Z.Q.; Khin, Z.; Peter, R.; Li, Y.Q.; Qu, X.M.; Song, S.H.; Peng, L.G.; Huang, J.J. Geology, Fluid Inclusions, and Oxygen Isotope Geochemistry of the Baiyinchang Pipe-Style Volcanic-Hosted Massive Sulfide Cu Depositin Gansu Province, Northwestern China. *Econ. Geol.* **2008**, *103*, 269–292.

12. Yu, J.Y.; Li, X.M.; Ma, Z.P.; Sun, J.M. Chronological study of meta-acidic volcanics in Qingshuigou-Bailiugou orefield, Qilian county of Qinghai province. *Adv. Earth Sci.* **2010**, *25*, 55–60. (In Chinese)

13. Xia, L.Q.; Xia, Z.C.; Ren, Y.X.; Zuo, G.C.; Qiu, J.X. *Volcanism and Mineralization of Qilian Mountain and Adjacent Area*; Geological Publishing House: Beijing, China, 1998. (In Chinese)

14. Ren, Y.X.; Peng, L.G.; Li, Z.P.; Li, X.M.; Luo, Y.P.; Yang, J.G. *Metallogenic Prediction and Optimizd Target Area of the Massive Sulfide Deposit of Qilian-Jinfosi, North Qilian Mountain*; Xi'an Institute of Geology and Mineral Resources: Xi'an, China, 1997; pp. 1–114. (In Chinese)

15. Xia, L.Q.; Xia, L.Q.; Ren, Y.X.; Xu, X.Y.; Yang, H.Q. *Tectonic-Volcanic Magmatism-Metallogenic Dynamics of North Qilian Mountain*; Geological Publishing House: Beijing, China, 2001; pp. 1–288. (In Chinese)

16. Peng, S.X.; Yin, C.M.; Liu, J.C.; Zhang, H.D. An Analytical Overview of the Precambrian Basement Properties, Source Area Characteristics of Volcanic Rocks and Some Prospecting Problems in the North Qilian Orogenic Belt. *Geol. Prospect* **2012**, *48*, 250–258. (In Chinese)

17. Xia, L.Q.; Xia, Z.C.; Ren, Y.X.; Xu, X.Y.; Peng, L.G.; Li, W.Y.; Yang, Z.P.; Zhao, D.H.; Song, Z.B.; Li, X.M. The paleosubmarine volcanism and mineralization in North Qilian mountains. *Acta Geosci. Sin.* **1999**, *20*, 259–264. (In Chinese)

18. Xu, X.Y.; He, S.P.; Wang, H.L.; Zhang, E.P.; Chen, X.L.; Sun, J.M. Tectonic framework of North Qinling mountain and North Qilian mountain conjunction area in early Paleozoic, A study of the evidences from strata and tectonic-magmatic events. *Northwestern Geol.* **2008**, *41*, 1–21. (In Chinese)

19. Mao, J.W. *Metallogenic Series and Metallogenic Evaluation of Cu-Fe-W Polymetallic Deposit in the West Section of North Qilian Mountain*; Geological Publishing House: Beijing, China, 2003. (In Chinese)

20. Zhang, R.L. *Early Paleozoic Marine Volcanic Sedimentary Facies and Geological Prospecting in North Qilian Mountains*; Geological Publishing House: Beijing, China, 1997. (In Chinese)

21. Peng, S.X.; Chen, J.L.; Cheng, J.X.; Yu, J.Y.; Zhang, S.N.; Zhang, H.D. Mineralization environment of the massive Fe-S type and Pb-Zn-Cu type sulfide deposits in Qingshuigou-Bailiugou, North Qilian, NW China. *Acta Geol. Sin.* **2013**, *87*, 1003–1012. (In Chinese)

22. Yan, Z.; Xiao, W.J.; Windley, B.F.; Wang, Z.Q.; Li, J.L. Silurian clastic sediments in the North Qilian Shan, NW China: Chemical and isotopic constraints on their forearc provenance with implications for the Paleozoic evolution of the Tibetan Plateau. *Sediment. Geol.* **2010**, *231*, 98–114. [CrossRef]

23. Yan, Z.; Xiao, W.; Wang, Z.; Li, J. Integrated analyses constraining the provenance of sandstones, mudston. *Can. J. Earth Sci.* **2007**, *44*, 961–986. [CrossRef]

24. Zhang, X.J.; Tao, M.X.; Dong, X.; Wei, X.H. Neotectonic movement and mineralization of the North Qilian area. *Northwestern Geol.* **2003**, *36*, 8–15. (In Chinese)

25. Peng, S.X.; Cheng, J.X.; Yu, J.Y.; Zhang, H.D.; Xiao, C.Y.; Hei, H. The Metallogenic Characteristic and Prospecting of the Massive Sulfide Deposit in Qingshuigou-Bailiugou Ore Field, North Qilian Mountain. *Northwestern Geol.* **2013**, *46*, 142–150. (In Chinese)

26. Li, W.Z.; Yuan, G.L.; Gong, Z.Y.; Gong, Z.Y.; Dong, L.; Li, Q. Tectonic Sense and Geochemical Behavior of Volcanic Rock in Xialiugou-xiagou Area of North Qilian Area. *Gansu Metall.* **2017**, *39*, 27–31. (In Chinese)

27. Guo, Y.R.; Jin, W. Characteristics and Forming Setting Analysis of Gadaban Kuroko-type Deposit in Northern Qilian. *Northwestern Geol.* **2014**, *47*, 191–197. (In Chinese)

28. Ren, Y.X. *Metallogenic Conditions and Predictions of Massive Sulfide Deposits in Qingguigou-Bailiugou ore Field in North Qilian Mountains*; Geological Publishing House: Beijing, China, 2000. (In Chinese)

29. Cao, D.Z.; Wang, Y.D.; Ma, Z.L.; Zhao, R.F. Geological characteristics and prospecting model of the Guomis-Gadaban metallogenic zone. *Northwestern Geol.* **2006**, *39*, 12–19. (In Chinese)

30. Brown, P.E. FLINCOR: A microcomputer program for the reduction and investigation of fluid-inclusion data. *Am. Mineral.* **1989**, *74*, 1390–1393.

31. Wang, S.; Li, B.; Zhang, X.K.; Wang, P.; Chao, W.W.; Ye, H.S.; Yang, Y.Q. Genesis of the Huoshenmiao Mo deposit in the Luanchuan ore district, China: Constraints from geochronology, fluid inclusion, and H–O–S isotopes. *Geosci. Front.* **2019**, *10*, 331–349. [CrossRef]

32. Yu, J.; Li, N.; Shu, S.P.; Zhang, B.; Guo, J.P.; Chen, Y.J. Geology, fluid inclusion and H-O-S isotopes of the Kuruer Cu-Au deposit in Western Tianshan, Xinjiang, China. *Ore Geol. Rev.* **2018**, 237–249. [CrossRef]

33. Clayton, R.N.; Mayeda, T.K. The use of bromine pentafluoride in the extraction of oxygen from oxides and silicates for isotopic analysis. *Geochim. Cosmochim. Acta* **1963**, *27*, 43–52. [CrossRef]

34. Friedman, I. Deuterium content of natural water and other substances. *Geochim. Cosmochim. Acta* **1953**, *4*, 89–103. [CrossRef]

35. Liu, Q.Q.; Shao, Y.J.; Li, D.F.; Luo, Z.Z. Processes and ore genesis at the Yaochong Mo deposit, Henan Province, China. *Ore Geol. Rev.* **2017**, *86*, 692–706. [CrossRef]

36. Zhang, Y.; Shao, Y.J.; Li, H.B.; Liu, Z.F. Genesis of the Xinqiao Cu-S-Fe-Au deposit in the Middle-Lower Yangtze River Valley metallogenic belt, Eastern China: Constraints from U-Pb-Hf, Rb-Sr, S, and Pb isotopes. *Ore Geol. Rev.* **2017**, *86*, 100–116. [CrossRef]

37. Roedder, E. Fluid inclusions. *Rev. Mineral.* **1984**, *12*, 644.

38. Lu, H.Z.; Fan, H.R.; Ni, P.; Ou, G.X.; Shen, K.; Zhang, W.H. *Fluid Inclusions*; Science Press: Beijing, China, 2004. (In Chinese)

39. Clayton, R.N.; O' Neil, J.R.; Mayeda, T.K. Oxygen isotope exchange between quartz and water. *J. Geophys. Res.* **1972**, *77*, 3057–3067. [CrossRef]

40. Sheppard, S.M.F. Characterization and isotopic variations in natural waters. *Rev. Mineral.* **1986**, *16*, 165–183.

41. Taylor, H.P. The application of oxyen and hydrogen isotope studies to problems of hydrothermal alteration and ore deposition. *Econ. Geol.* **1974**, *69*, 843–883. [CrossRef]

42. Zartman, R.E.; Doe, B.R. Plumbotectonics-the model. *Tectonophysics* **1981**, *75*, 135–162. [CrossRef]

43. Huston, D.L. Stable isotopes and their significance for understanding the genesis of volcanic-hosted massive sulfide deposits: A review. *Rev. Econ. Geol.* **1999**, *10*, 151–180.

44. Xia, L.Q.; Li, X.M.; Yu, J.Y.; Wang, G.Q. Mid-Late Neoproterozoic to early Paleozoic vclcanism and tectonic evolution of the Qilian mountain. *Geol. China* **2016**, *43*, 1087–1138. (In Chinese)

45. Cong, Z.C. Study on Metallogenic Regularity of Copper Polymetallic Deposit in the North Qilian, Qinghai. Ph.D. Thesis, Jilin University, Jilin, China, 2017. (In Chinese).

46. Kamprad, J. Zonation of alteration facies at Western Taarsis: Implications for the genesis of Cu-Au deposits, Mount Lyell field, western Tasmania. *Econ. Geol.* **2001**, *96*, 1123–1132.

47. Huston, D.L.; Relvas, J.M.R.S.; Gemmell, J.B.; Drieberg, S. The role of granites in volcanic-hosted massive sulphide ore-forming systems: An assessment of magmatic-hydrothermal contributions. *Miner. Depos.* **2011**, *46*, 473–507. [CrossRef]

48. De Ronde, C.E.J. Fluid chemistry and isotope characteristics of seafloor hydrothermal systems and associated VMS deposits: Potential for magmatic contributions. *Magmas Fluids Ore Depos.* **1995**, *23*, 479–509.

49. Bodnar, R.J.; Lecumberri-Sanchez, P.; Moncada, D.; Steele-MacInnis, M. Fluid inclusions in hydrothermal ore deposits. In *Treatise on Geochemistry*, 2nd ed.; Holland, H.D., Turekian, K.K., Eds.; Elsevier: Amsterdam, The Netherlands, 2014; pp. 119–143.

50. Zhou, T.F.; Qiu, S.C.; Liu, Y.; Xu, X.C.; Xiong, C.L. Preliminary studies on ore-forming process of the palaeozoic copper deposits in southern zoulang mountains, Gansu. *Geol. Anhui* **1998**, *2*, 21–24. (In Chinese)

51. Du, Z.Z. Research on Mineralization of the BaiYinchang Copper Multimetal Field, GanSu Province, China. Ph.D. Thesis, China University of Geosciences, Beijing, China, 2014. (In Chinese).

52. Liang, W.J.; Yan, G.S.; Li, J.C.; Zuo, C.Q.; Du, Z.Z.; Zhen, S.J.; Zhang, Z.H.; Li, Y.S. Characteristics of fluid inclusions of the Xiaotieshan lead Zinc polymetallic deposit in Gansu province. *Bull. Mineral. Petrol. Geochem.* **2016**, *35*, 317–327. (In Chinese)

53. Ohmoto, H. Formation of volcanogenic massive sulfide deposits: The Kuroko perspective. *Ore Geol. Rev.* **1996**, *10*, 135–177. [CrossRef]

54. Ohmoto, H. Systematics of sulfur and carbon isotopes in hydrothermal ore deposits. *Econ. Geol.* **1972**, *67*, 551–578. [CrossRef]

55. Wu, J.R. Analysis of Geologic Characteristics and Ore-Forming Conditions of Pyritic-Copper-Polymetallic Deposits in Baiyinchang Orefield, Gansu. *Northwest Geosci.* **1992**, *2*, 83–96. (In Chinese)

56. Cheng, X.H.; Xu, J.H.; Wang, J.X.; Chu, H.X.; Xiao, X.; Zhang, H. Sulfur and lead isotope constrains on source of ore-forming materials in Asmara VMS-type deposits, Eritrea. *Chin. J. Nonferrous Met.* **2017**, *27*, 795–810. (In Chinese)

57. Zeng, Z.G.; Jiang, Q.F.; Zhai, S.K.; Qin, Y.S. Lead isotopic compositions of massive sulfides from the Jade hydrothermal field in the Okinawa Trough and its geological implications. *Geochimica* **2000**, *29*, 239–245. (In Chinese)

58. Dai, B.Z.; Zhao, K.D.; Jiang, S.Y. Modern Sea-floor Hydrothermal Activity and Genesis of Massive Sulfide Deposits: An Overview. *Bull. Mineral. Petrol. Geochem.* **2004**, *23*, 246–253. (In Chinese)

59. Jiang, S.Y.; Yang, T.; Li, L.; Zhao, K.D.; Ling, H.F. Lead and sulfur isotopic compositions of sulfides from the TAG hydrothermal field, Mid-Atlantic Ridge. *Acta Petrol. Sin.* **2006**, *22*, 2597–2602. (In Chinese)

60. Petersen, S.; Herzig, P.M.; Hannington, M.D. Third dimension of a presently forming VMS deposit: TAG hydrothermal mound, Mid-Atlantic Ridge, 26°N. *Miner. Deposita* **2000**, *35*, 233–259. [CrossRef]

61. Lode, S.; Piercey, S.J.; Layne, G.D.; Piercey, G.; Cloutier, J. Multiple sulphur and lead sources recorded in hydrothermal exhalites associated with the Lemarchant volcanogenic massive sulphide deposit, central Newfoundland, Canada. *Miner. Deposita* **2016**, *52*, 1–24. [CrossRef]
62. Wang, Y.; Qian, Q.; Liu, L.; Zhang, Q. Major geochemical characteristics of bimodel volcanic rocks in different geochemical environments. *Acta Petrol. Sin.* **2000**, *16*, 169–173. (In Chinese)